ACCSCIENCE PUBLISHING

International Journal of Bioprinting

RESEARCH ARTICLE

Integrated 3D printing of cementless CoCrMo femoral condyles optimizes trabecular surfaces and material performance

Jiawei Wu[1†], Zhiwei Zhou[1†], Tianbai Yu[1,2], Wei Wang[1], and Brian Y. Chang[3,4*]

[1]Suzhou Microport Orthorecon Co., Ltd., Suzhou, Jiangsu, China

[2]School of Health Science and Engineering, University of Shanghai for Science & Technology, Shanghai, China

[3]Institute for Medical Engineering and Science, Massachusetts Institute of Technology, Cambridge, MA, United States of America

[4]Miracle Point Global LLC, Irvine, CA, United States of America

(This article belongs to the *Special Issue*: *3D-Printed Biomedical Devices*)

Abstract

Conventional cementless femoral condyles in artificial knee systems are commonly manufactured by casting followed by a surface treatment using plasma spraying or metallic sintering. However, both techniques suffer from weak coating-substrate interfaces that contribute to early loosening and higher revision rates. To overcome this limitation, we employed integrated 3D printing (I3P), an additive manufacturing strategy based on laser powder bed fusion, to fabricate monolithic cobalt-chromium-molybdenum femoral condyles with trabecular-inspired porous architectures. Compared with cast-sintered counterparts, I3P substrates exhibited refined microstructures and superior mechanical performance after hot isostatic pressing, reaching a yield strength of 637.33 MPa, ultimate tensile strength of 1140.00 MPa, and elongation of 27.33%. The I3P femoral condyles also showed enhanced fatigue resistance, withstanding 10 million cycles under a 3000 N load, and demonstrated improved wear behavior against ultrahigh-molecular-weight polyethylene liners. Furthermore, the trabecular-inspired lattice achieved stronger integration with the substrate than sintered coatings, with tensile and shear strengths of 56.09 and 49.97 MPa, respectively. Together, these findings establish I3P as a robust manufacturing strategy that integrates substrate and surface in a single step, enabling the production of durable, osteointegrative femoral condyles with significant potential to improve implant longevity and clinical outcomes in knee joint reconstruction.

Keywords: Additive manufacturing; Cementless femoral condyles; Cobalt-chromium-molybdenum alloys; Fatigue and wear resistance; Integrated 3D printing; Osteointegration; Total knee arthroplasty; Trabecular surface architecture

†These authors contributed equally to this work.

***Corresponding author:**
Brian Y. Chang
(bychang@mit.edu)

Citation: Wu J, Zhou Z, Yu T, Wang W, Chang BY. Integrated 3D printing of cementless CoCrMo femoral condyles optimizes trabecular surfaces and material performance. *Int J Bioprint*. 2026;12(1):371-384. doi: 10.36922/IJB025380389

Received: September 19, 2025
Revised: November 1, 2025
Accepted: November 3, 2025
Published online: November 11, 2025

1. Introduction

Total knee arthroplasty (TKA) is one of the most effective surgical treatments for end-stage knee disorders, such as osteoarthritis, rheumatoid arthritis, and post-traumatic arthritis,

aiming to relieve pain, correct deformities, and restore joint function.[1–3] The procedure involves the implantation of artificial joint components, primarily a femoral condyle implant that replaces the load-bearing surface of the distal femur. As TKAs are increasingly performed in younger and active patients with higher expectations for postoperative mobility, long-term prosthesis durability and stability have become crucial.[4] The clinical success of cementless femoral condyle implants hinges on osseointegration, where host bone forms a strong biomechanical interface with the implant to ensure durable fixation and mechanical stability.

To facilitate this, standardized femoral condyle implants are traditionally manufactured in a two-step process. First, cobalt-chromium-molybdenum (CoCrMo) alloy is cast to form the bulk geometry of the femoral condyle. The resulting surface is smooth and biologically inert, limiting osseointegration. Therefore, a secondary surface treatment is applied to create a trabecula-inspired porous structure that is conducive to osseointegration. The trabecular structure promotes bone in-growth that forms the strong biomechanical interface that ensures durable fixation.[5,6] Modern surface modification treatments can be done by plasma-spraying coatings or, more commonly, sintering coatings.[7,8]

Plasma-spraying is a widely used surface modification technique for cementless implants, in which metallic or bioactive ceramic particles, such as hydroxyapatite (HA), are propelled onto the implant surface to create the porous, textured coating. However, plasma-sprayed coatings rely primarily on mechanical interlocking rather than metallurgical bonding, which results in relatively low interfacial strength and increases the risk of delamination under cyclic loading. In addition, HA coatings, while bioactive, are susceptible to long-term degradation, which can further compromise mechanical stability over time.[9–11] Examples of current commercial designs include cementless femoral condyles with a cast CoCrMo substrate and dual plasma-sprayed coatings of HA and pure titanium (Chunli Medical, China), as well as designs featuring a single-layer plasma-sprayed titanium coating (JUST Medical, China).

Sintering is a more common surface modification technique used to enhance osseointegration in cementless implants. Metallic beads or particles are bonded to the implant surface at high temperatures, promoting atomic diffusion between the coating and the substrate. This metallurgical bonding results in stronger and more stable interfaces compared to plasma-sprayed coatings. However, the high-temperature sintering process can lead to grain coarsening in the underlying metallic substrate, potentially reducing its mechanical properties. Additionally, sintering requires longer production cycles, limiting manufacturing efficiency.[12,13] Commercial examples include femoral condyles with cast CoCrMo substrates and dual-layer surfaces composed of sintered CoCrMo beads combined with a HA solution-deposited coating (Triathlon Tritanium, Stryker, USA). Another design features a dual plasma-sprayed coating of pure titanium and calcium phosphate (e.motion, B. Braun, Germany).

The compromises of traditional manufacturing TKA implants stem from requiring two steps to manufacture a mechanically stable bulk geometry via casting with a biocompatible surface that promotes osseointegration via a subsequent surface treatment. In contrast, additive manufacturing techniques, such as 3D printing may pose a solution without these compromises. CoCrMo alloys produced by 3D printing are widely used in dental prosthetics, but their application in cementless knee implants remains limited. Laser powder bed fusion (LPBF) is among the most established technologies in metal additive manufacturing.[14,15] The process begins with a computer-aided design CAD model which is then segmented into a sequence of thin two-dimensional layers. On the build platform, a recoater blade or roller spreads a fine layer of metal powder (typically 20–60 μm). A high-power fiber laser selectively scans the powder bed according to the sliced geometry, fully melting the particles to form dense metallurgical bonds. After each layer is consolidated, the platform lowers by one layer thickness, new powder is deposited, and the next layer is fused to the previous one. This cycle is repeated until the entire part is completed.[16–18] Upon completion, the component is removed from the powder bed, excess powder and support structures are eliminated, and postprocessing such as heat treatment, wire cutting, or finishing may be performed. A unique advantage of LPBF is the ability to precisely control porosity, pore size, strut thickness, therefore allowing it to produce dense substrates as well as precise trabecula-inspired lattices.[19–21]

Consequently, LPBF can be adapted to replace the traditional two-step casting and surface treatment by manufacturing a stable bulk geometry and a porous trabecula-inspired surface layer in a single step known as integrated 3D printing (I3P). Unlike traditional LPBF, I3P simultaneously prints the CoCrMo substrate and trabecular lattice with the same process. I3P reduces manufacturing steps and achieves stronger bonding between the porous lattice and the metallic base when compared with traditional sintering or plasma spraying.[22] To date, I3P has been primarily applied in complex anatomical reconstructions and revision TKA procedures where patient-specific customization is essential.[23] However, with the maturation of additive manufacturing, standardized I3P manufactured cementless femoral

condyle implants are expected to achieve broader clinical adoption in primary TKA procedures.[24–26]

In this study, we employed I3P techniques to fabricate the design of a standardized commercially available femoral condyle implant (EVOLUTION, MicroPort Orthopedics, USA). Comparative analyses were performed against the conventionally manufactured implant that uses a sintered surface treatment. The evaluation focused on raw material characteristics, as well as the fatigue and wear performance of the implants. In addition, the tensile and shear tests were conducted specifically to quantify the interfacial bonding strength between the trabecular-inspired lattice layer and the CoCrMo substrate. These assessments collectively confirmed the advantages and feasibility of standardized I3P-fabricated cementless femoral condyles, offering a novel solution for future primary TKAs.

2. Materials and methods

To enable direct comparison with conventional commercially available implants, femoral condyles of identical geometric design were fabricated using I3P. Experimental evaluation was divided into two components: (i) the substrate material, representing the traditionally cast bulk CoCrMo alloy; and (ii) the surface material, representing the porous layer typically applied via plasma spraying or sintering in conventional manufacturing. This approach allowed for independent assessment of the intrinsic material properties and interfacial performance associated with each manufacturing strategy.

2.1. Materials

ASTM F75 compliant CoCr02 cobalt-chromium-molybdenum alloy powder (AVIC Maite Additive Manufacturing Technology, Beijing, China) was used as the raw I3P material. The powder was produced using gas atomization via nonvacuum induction melting (Table 1).

Table 1. Chemical composition and physical properties of CoCr02 cobalt-chromium-molybdenum alloy powder used as the raw material for manufacturing by integrated 3D printing

Properties		Results
Chemical composition	C	0.161%
	N	0.12%
	Si	0.63%
	Mn	0.44%
	Ni	0.24%
	Fe	0.49%
	Cr	27.10%
	Mo	5.60%
	B	0.004%
	Co	Balance
Physical properties	Particle size	D10: 17.01 μm D50: 28.94 μm D90: 48.51 μm
	Apparent density	4.7 g/cm³
	Tap density	5.4 g/cm³
	Hall flowmeter	13.6 s/50g

Notes: The powder was produced by gas atomization through nonvacuum induction melting (AVIC Maite Additive Manufacturing Technology, Beijing, China). These baseline characteristics establish material compliance and quality for subsequent femoral condyle fabrication.

2.2. Sample preparation

2.2.1. Integrated 3D printing process

The specimens were produced using a BLT S310 LPBF system (Xi'an Bright Laser Technologies, China) with 30 μm layer thickness, 160 W laser power, a scanning speed of 800 mm/s, and a laser spot size of 100 μm. During fabrication, the build chamber was purged with argon to maintain an oxygen concentration below 0.1%. The external geometry of the I3P-fabricated products was identical to that of a commercially available cast and sintered femoral condyle (*EVOLUTION,* MicroPort Orthopedics, USA). The trabecular-inspired porous structures were designed using Autodesk Within (Autodesk Inc., USA), with target pore size pf 0.75 mm, trabecular topology, and a 0.2 mm uniform strut thickness. The model was exported in STL format and subsequently sliced using BLT BP software (BLT, China), where parameters such as layer thickness, laser power, and scanning speed were defined and controlled. The total thickness of trabecular-inspired porous structures was 700–1000 μm, which is similar to that of the traditionally manufactured counterparts.

After I3P, the samples were separated from the build plate by wire electrical discharge machining. Postprocessing included hot isostatic pressing (HIP), carried out at 1167°C and 135 MPa for 4 h in an argon atmosphere, followed by vacuum quenching (WuXi Falcon Advanced Materials Technology, China). This process mirrors the process-processing performed on commercially available traditionally manufactured implants. The HIP-treated products were then finish-machined for testing. The parameters adopted in this study represent a relatively optimized scheme based on comprehensive considerations. Specimen for tensile and trabecular interfacial bonding tests were prepared under the same design and processing conditions as the implant. For comparative purposes, additional tensile specimens were fabricated using the identical I3P parameters but without HIP treatment.

2.2.2. Traditional casting-sintering

The cast and sintered cementless femoral condyles (EVOLUTION, MicroPort Orthopedics, USA) were directly obtained from commercial sources. According to the manufacturer, the implant is manufactured using a CoCrMo bead-sintering surface treatment. Following sintering, the components underwent the same HIP treatment as the I3P specimens. Specimens for tensile and trabecular interfacial bonding tests were prepared under identical design and processing parameters as the commercial implants.

2.3. Substrate material testing

2.3.1. Tensile testing

Tensile testing was conducted in accordance with ASTM E8/E8M using a SUNS UTM 5205X universal testing machine. The specimens had a total length of 92 mm, with a gauge diameter of 6 mm and a gauge length of 36 mm, and were prepared in the form of cylindrical round bars. For each group, five specimens were tested from the cast substrate, the I3P substrate before HIP, and the I3P substrate after HIP. The tests were performed under displacement control at a crosshead separation rate of 2.54 mm/min, and continued until specimen failure. The following mechanical properties were recorded: 0.2% offset yield strength (Rp0.2), ultimate tensile strength, and elongation at fracture. From the recorded data, means and sample standard deviations were computed. Statistical significance was evaluated using two-sample, two-tailed Student's *t*-tests.

2.3.2. Microstructure evaluation

Microstructural observations were performed in accordance with ISO 643 using a NIKON LV150N upright metallographic microscope. The specimens were sectioned from the tensile bars. Electrical discharge machining was employed to cut sections both parallel and perpendicular to the build direction, which were then prepared for microstructural examination. The specimens were mounted using hot compression mounting, followed by sequential grinding with SiC abrasive papers ranging from 180# to 2000# grit, progressing from coarse to fine. Polishing was then carried out on a metallographic polishing machine until the surfaces were free of visible scratches, after which the samples were rinsed and air-dried. To clearly reveal the grain boundaries, carbide phases, and matrix microstructure of the CoCrMo alloy, the polished surfaces were etched with a mixed acid solution consisting of 20 mL of 37% hydrochloric acid and 1 mL of 30% hydrogen peroxide. In addition, a scanning electron microscope (Prisma E with Xflash Detector 630M, Thermo Fisher Scientific, USA) was employed for further magnified analyses of the black spots observed in the microstructure

2.3.3. Wear testing

Femoral condyle accelerated wear testing was conducted in accordance with ISO 14243-3 using a Jointwear-K4301 knee wear simulator (Shanghai Aose Inspection Technology Co., Ltd, China). For each group (I3P and CS), three femoral condyles were tested. During testing, the femoral condyles were articulated with compatible commercially available tibial tray and tibial insert (MicroPort Orthopedics, USA). Prior to testing, all specimens were cleaned and dried according to the standard procedure. Calf serum was used as the lubricant during the wear simulation. Specimens were removed, weighed using an electronic balance, and the lubricant was replaced every 500,000 cycles before resuming the test. At each 500,000-cycle interval, for each group (I3P and CS), the mean and sample standard deviation of the measurements were calculated. The wear simulation was continued until either 5 million cycles were completed or surface failure occurred, whichever came first.

2.3.4. Fatigue testing

Fatigue testing was conducted in accordance with ASTM F3210 and carried out using an Instron fatigue testing machine (Instron Corporation, USA). Prior to testing, following ASTM F3161, finite element analysis (FEA) located the maximum principal-stress point within the condyle bisection-plane region. The embedding position was set 4.5 mm below this point, as shown in Figure 1. Embedded femoral condyle assemblies were then mounted on the testing machine for fatigue evaluation. The loading head of the tester was positioned on the highest point of the posterior femoral condyle. A sinusoidal cyclic load starting from 2300 N was applied with a load ratio of R = 0.1 and a frequency of 15 Hz. A step-loading method was employed to test a series of femoral components. The test was terminated when either 10 million cycles were reached or specimen failure occurred. At each loading stage, three specimens per group (CS and I3P) were tested. For each group, the mean and sample standard deviation were computed, and results were plotted on a logarithmic scale. Error bars correspond to the logarithm of the mean plus or minus one standard deviation (*i.e.*, log(mean ± SD)).

2.4. Methods for surface material testing

2.4.1. Porosity evaluation

The morphology of the trabecula-inspired lattice structures was characterized using an industrial CT scanner (Nikon XTH225) with a scanning resolution of 8 μm. During testing, the X-ray source voltage and current were adjusted to generate beams of appropriate energy to penetrate the

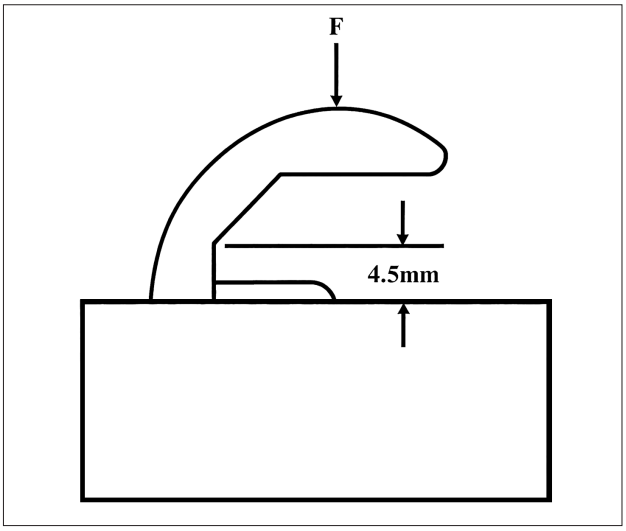

Figure 1. Schematic for fatigue testing of cementless femoral condyles. Specimens were embedded in dental stone and mounted in an Instron fatigue testing machine with cyclic loading applied to the posterior condyle. This preparation enabled controlled evaluation of long-term mechanical performance under simulated gait conditions.

porous metallic specimens. The transmitted signals were collected by the detector, converted into digital data, and reconstructed into computed tomography (CT) images through computational projection algorithms.

Subsequently, image segmentation, 3D reconstruction, region growing, and quantitative statistical analysis using a Gaussian model were performed to determine morphological parameters, including porosity, pore size, and strut thickness of the tested structures.

2.4.2. Tensile testing

Tensile testing of the trabecula-inspired porous structures was conducted in accordance with ASTM F1147 using a SUNS UTM 5205X universal testing machine. Ten specimens were prepared each for the sintered substrate bars and the I3P substrate bars. Prior to testing, the porous surface of each specimen was bonded to a flat substrate of the same base material using an adhesive with a tensile strength of not less than 34.5 MPa.

Both the porous-coated substrate bars and the flat substrate bars had a cross-sectional area of 5.07 cm^2. During testing, the tensile load was applied perpendicular to the plane of the trabecula-inspired porous structures at a constant crosshead speed of 0.25 cm/min, and was continued until failure occurred at the bonded interface. Strength data for each group were summarized and analyzed using box-and-whisker plots. Statistical significance was evaluated using two-sample, two-tailed Student's *t*-tests.

2.4.3. Shear testing

Shear testing of the trabecula-inspired porous structures was conducted in accordance with ASTM F1147 using a SUNS UTM 5205X universal testing machine. Ten specimens were prepared each for the CS substrate bars and the I3P substrate bars. Prior to testing, the porous surface of each specimen was bonded to a flat substrate of the same base material using an adhesive with a tensile strength of not less than 34.5 MPa.

Both the porous-coated substrate bars and the flat substrate bars had a cross-sectional area of 2.84 cm^2. During testing, the shear load was applied parallel to the plane of the trabecula-inspired porous structures at a constant crosshead speed of 0.25 cm/min, and loading continued until failure occurred at the bonded interface. Strength data for each group were summarized and analyzed using box-and-whisker plots. Statistical significance was evaluated using two-sample, two-tailed Student's *t*-tests.

3. Results

3.1. Substrate material

For a femoral condyle, the mechanical properties of the substrate material determine its resistance to failure during service and critically influence its overall performance. Tensile properties are the most representative indicators of comprehensive mechanical behavior and are strongly correlated with the underlying microstructure of the raw material. Thus, the tensile properties and microstructures of CoCrMo alloys from I3P (pre- and post-HIP) and conventionally cast femoral condyles were directly compared (Figure 2).

Conventionally cast CoCrMo substrate tensile testing result in a yield strength of 523.33 ± 12.92 MPa, a tensile strength of 786.00 ± 41.67 MPa, and an elongation at fracture of 14.33 ± 0.24%. I3P-manufactured CoCrMo substrate yielded mixed material characteristics prior to HIP with a yield strength of 508.38 ± 9.88 MPa, an ultimate tensile strength of 922 ± 9.57 MPa, and an elongation at fracture of 8.83 ± 2.25%. However, I3P substrate characteristics were superior to casting following HIP with a yield strength of 637.33 ± 1.70 MPa, a tensile strength of 1140.00 ± 31.82 MPa, and an elongation at fracture of 27.33 ± 4.99%.

This phenomenon corresponds with microscopic findings (Figure 2). Prior to HIP, the I3P substrate contained numerous micropores (Figure 2F). Pores were less pronounced on the planes perpendicular to the laser direction than on those parallel to it, suggesting they may originate from incomplete interlayer fusion during the additive manufacturing process (Figure 2A and 2B). The presence of these micropores may result in

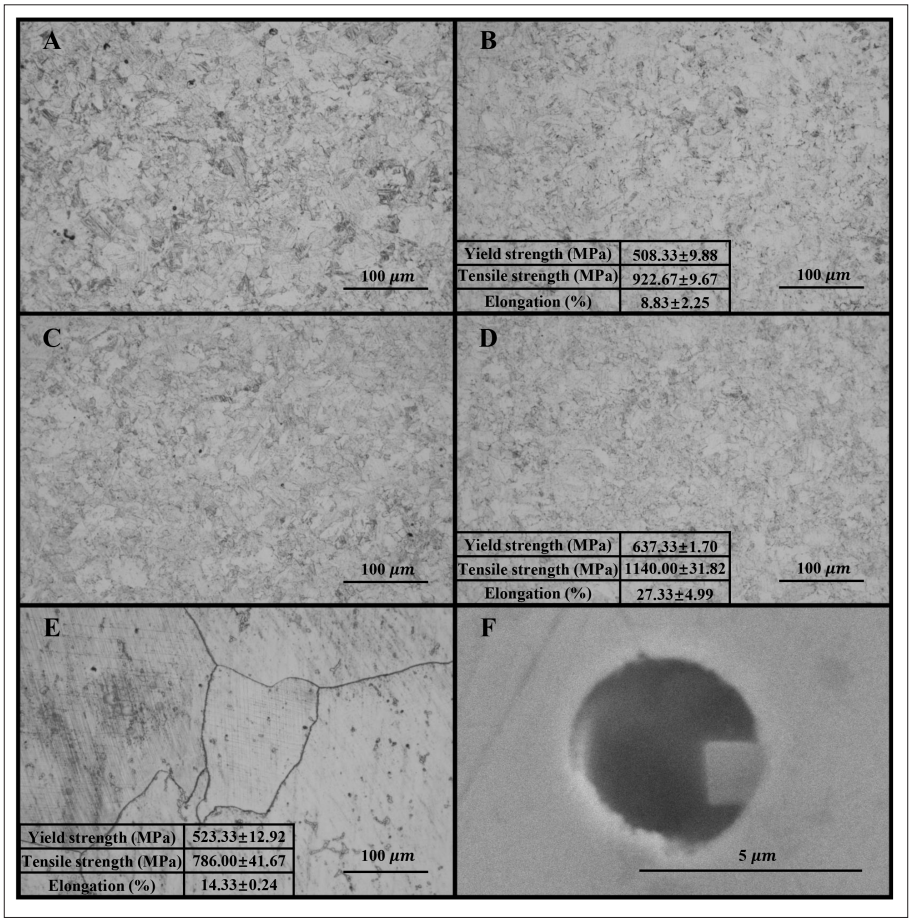

Figure 2. Microstructure and tensile properties of CoCrMo substrates manufactured by I3P and CS. (A,B) I3P substrate before HIP showing numerous micropores, more pronounced parallel to the laser direction (A) than perpendicular to it (B), which corresponded with reduced ductility (elongation: 8.8 ± 2.3%). (C,D) I3P substrate after HIP showing substantial pore elimination in both orientations, resulting in markedly improved mechanical performance (yield strength: 637 ± 1.7 MPa; UTS: 1140 ± 31.8 MPa; elongation: 27.3 ± 5.0%). (E) CS substrate after HIP exhibiting coarser grains and lower overall strength (yield strength: 523 ± 12.9 MPa; UTS: 786 ± 41.7 MPa; elongation: 14.3 ± 0.2%) compared with I3P after HIP. *HIP-treated I3P specimens demonstrated significantly superior properties compared with CS specimens, with two-sample Student's *t*-test *p*-values of 1.16×10^{-7}, 8.67×10^{-7}, and 8.19×10^{-4} for yield strength, tensile strength, and elongation, respectively. (F) Enlarged SEM micrograph highlighting residual micropores (black spots) prior to HIP. Abbreviations: HIP: Hot isostatic pressing; I3P: integrated 3D printing; SEM: Scanning electron microscopy; UTS: Ultimate tensile strength; CS: cast-sintered.

tensile properties inferior to those of the HIP-treated cast substrate. After HIP, however, such defects were largely eliminated in both orientations (Figure 2C and 2D), and combined with the refined microstructure, led to the post-HIP I3P substrate outperforming the cast substrate.

In summary, HIP not only improves the mechanical performance but also the structural stability of I3P materials, enabling I3P femoral condyles to exhibit superior properties compared with their conventionally cast counterparts.

3.2. Implant performance

During *in vivo* service, the implant is subject to long-term wear and cyclic fatigue stresses, which are a consequence of substrate material characteristics. Each gait cycle imposes frictional wear stress on the articulating surface and fatigue stresses on the entire femoral condyle. Wear and fatigue resistance are consequently two critical determinants of the prosthesis's long-term functionality and revision rate.

Wear resistance was quantified by measuring mass loss every 500,000 cycles, up to 5,000,000 cycles, during articulated wear testing of three samples each from the post-HIP I3P manufactured and cast substrates. The I3P-manufactured femoral condyle demonstrated superior wear resistance with reduced change in mass (Figure 3) and superior hardness (31 Rockwell Hardness C scale (HRC) vs. 23 HRC). This advantage can be attributed to

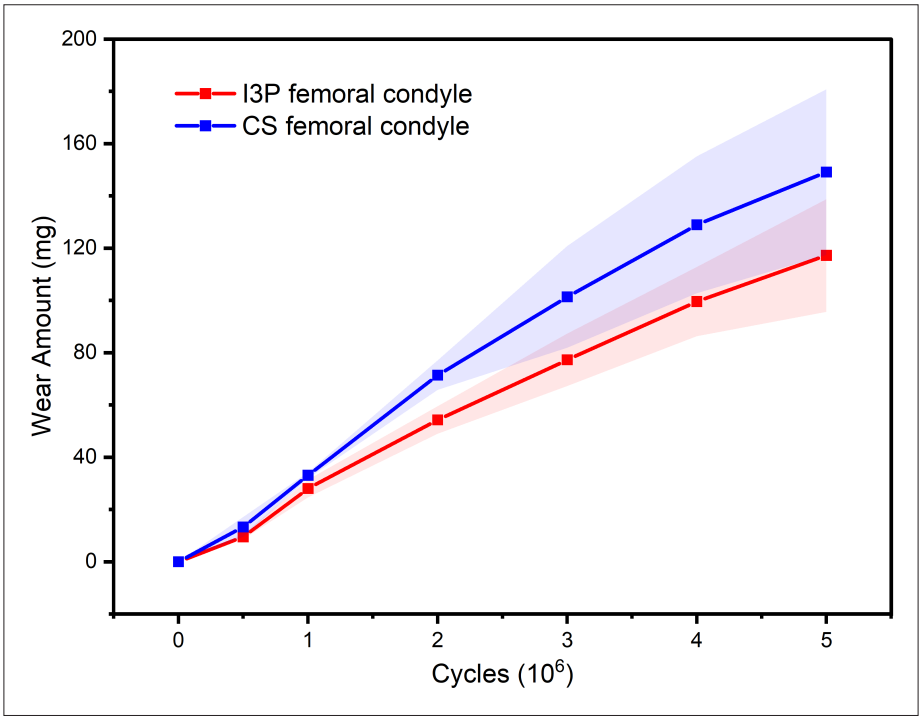

Figure 3. Wear resistance of I3P and CS cementless CoCrMo femoral condyles. Wear testing was performed for three specimens per group, with mass measured every 500,000 cycles up to 5,000,000 cycles of articulated motion. I3P femoral condyles demonstrated reduced mass loss compared with cast counterparts, consistent with their higher hardness (31 vs. 23 HRC) and finer, more homogeneous microstructure. These characteristics enabled smoother polishing and less counterface wear, resulting in superior overall wear performance of the coupled system. Abbreviations: CS, Cast-sintered; I3P, Integrated 3D printing.

the finer and more homogeneous grain structure of the I3P material, which provides higher hardness.

Fatigue resistance was evaluated by applying increasing sinusoidal cyclic loads in a step-loading method starting from 2300 N until implant failure or until a maximum of 10,000,000 cycles in seven groups of each manufacturing type. The I3P femoral condyle demonstrated superior fatigue resistance by surviving to the maximum load cycle up to 3000 N compared to 2900 N for the cast femoral condyle (Figure 4). Furthermore, the I3P femoral condyle maintained a trend of surviving a higher number of cycles for each subsequent increase in cyclic load (Figure 4). This superior performance can also be attributed to the homogeneity of the I3P substrate and its refined microstructural morphology, which enable more uniform distribution and transmission of applied stresses, thereby enhancing overall fatigue resistance.

The I3P femoral condyle demonstrated superior wear performance and fatigue resistance potentially due to finer and more homogeneous microstructure, an outcome that is consistent with the inherent material benefits of the I3P manufacturing approach.

3.3. Trabecular surface material

An essential feature of a cementless femoral condyle implant is its bone-contacting surface, which interfaces with host bone through a trabecula-inspired porous structure. The evaluation concerns two aspects: (i) connectivity and pore size distribution, which influence osteointegration, and (ii) bonding strength with the substrate, which influences durability and mechanical stability. In this comparison, the trabecular layer thickness of I3P products was controlled within the same range as sintered counterparts (700–1000 μm).

The connectivity and pore size of I3P-produced trabeculations was directly compared with that generated in a traditional sintering process through CT imaging. Connectivity was quantified by evaluating the lattice structure, I3P produced thinner struts (mean diameter 190.7 ± 44.3 vs. 247.6 ± 27.2 μm) with higher porosity (67.6% vs. 40.5%) (Figure 5A and 5C), characteristics conducive to promote osteointegration. The pore characteristics themselves were also measured with I3P yielding a mean pore size of 317.2 ± 124.4 μm and sintering yielding a mean pore size of 141.6 ± 49.2 μm (Figure 5B and 5D). Although the optimal pore

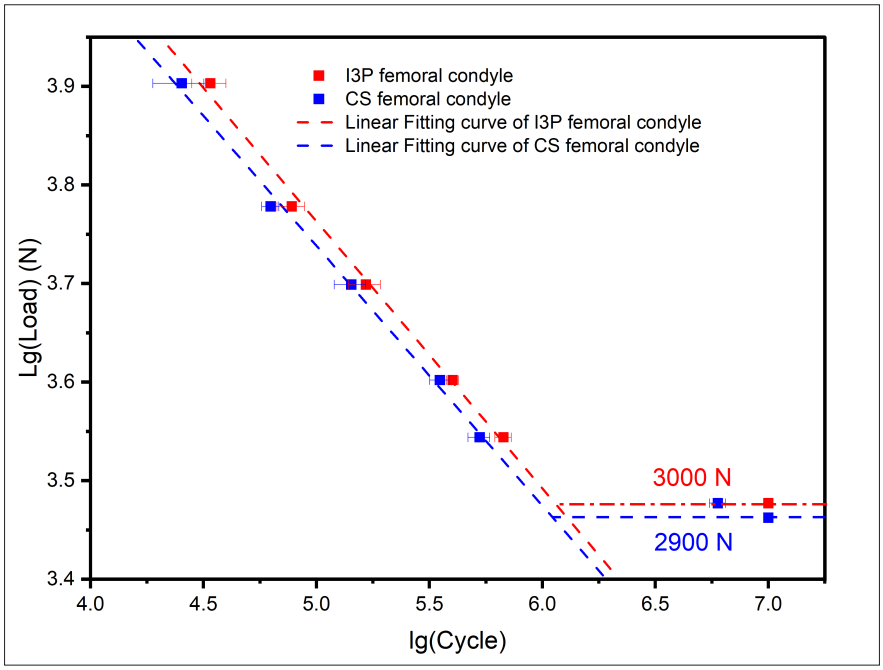

Figure 4. Fatigue performance of I3P and CS cementless CoCrMo femoral condyles. Seven specimens per group were tested using a step-loading protocol with sinusoidal cyclic loading (R = 0.1, 15 Hz), beginning at 2300 N and continuing until failure or 10 million cycles. I3P femoral condyles consistently survived more cycles at each load step and reached a maximum endurance of 3000 N, compared with 2900 N for cast counterparts. Superior performance is attributed to the finer grain structure and more homogeneous microstructure of I3P, which enable more uniform stress distribution and enhanced fatigue resistance. Abbreviations: CS, Cast-sintered; I3P, integrated 3D printing.

size for bone ingrowth is generally considered to be within 100–500 μm,[27] a broader pore size distribution is more favorable for accommodating different stages of osteointegration.[28–31]

Bond strength between the substrate and trabeculated surface layer was evaluated using a universal testing machine with 10 specimens each of I3P-produced and traditional sintered parts. I3P parts exhibited superior tensile strength (56.1 MPa) and shear strength (50.0 MPa) exceeding that of the sintered components (Figure 6), suggesting the superiority of producing the implant in a single step. Consequently, I3P provides a more durable and reliable bonding interface, establishing a level of structural stability that is difficult to achieve with conventional sintering techniques.

In summary, compared to conventional sintering, I3P yields a trabecular layer with higher porosity, more favorable pore size distribution, and stronger bonding to the substrate. These combined characteristics support more effective osteointegration while also providing superior mechanical stability, underscoring the advantages of I3P as a next-generation approach for cementless femoral condyle implants.

4. Discussion

As an emerging manufacturing technology, additive manufacturing provides remarkable advantages for fabrication of cementless femoral condyles. Yet most current implementations adopt a hybrid architecture in which a trabecular lattice is printed and then welded or brazed to a cast substrate (Longility, Abonisi Medical Technology). Compared with conventional sintered coating, 3D printing enables precise control of porosity, pore size, and 3D interconnectivity, thereby creating a microenvironment closer to human cancellous bone. However, the welded or brazed interface constitutes a mechanical weak link and a likely site for fatigue-crack initiation under the cyclic loads of daily walking and running, and the cast substrate is not readily patient-specific. In addition, a nonbiomimetic femoral condyle has been manufactured using additive manufacturing for complex clinical cases (Beijing Naton Medical Technology), but this approach does not fully exploit the advantages of 3D-printed trabecular architectures.

In contrast, the I3P strategy investigated in this study leverages the distinctive strengths of additive manufacturing to realize a truly monolithic, biomimetic design. The critical difference is I3P produces the

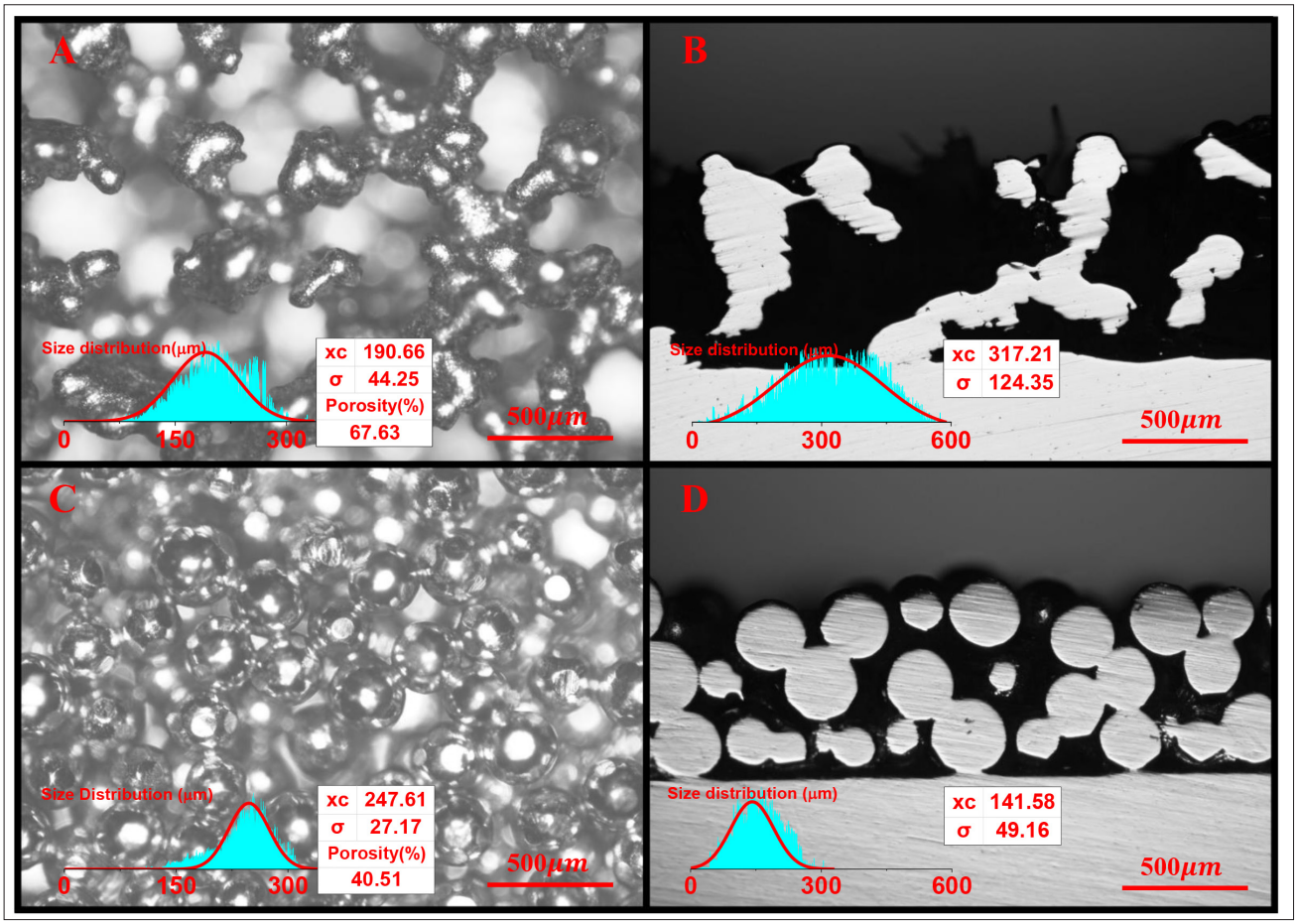

Figure 5. Trabecula-inspired lattice and pore characteristics of I3P and CS femoral condyles. (A) I3P lattice morphology with strut size distribution and Gaussian fitting. I3P struts were thinner (mean diameter: 190.7 ± 44.3 μm) and exhibited a broader size distribution, closely mimicking the heterogeneity of natural trabeculae. (B) I3P pore morphology with pore size distribution and Gaussian fitting. I3P generated larger pores (mean: 317.2 ± 124.4 μm) with a wider distribution, favorable for staged bone ingrowth. (C) CS lattice morphology with size distribution and Gaussian fitting. CS struts were thicker (mean: 247.6 ± 27.2 μm), less variable, and yielded lower overall porosity (40.5% vs. 67.6% in I3P), limiting osteointegration potential. (D) CS pore morphology with pore size distribution and Gaussian fitting. CS pores were smaller (mean: 141.6 ± 49.2 μm) and more narrowly distributed, reflecting limited controllability from bead-packing and sintering. All Gaussian fittings were performed without normalization and with the baseline parameter fixed at 0. Collectively, I3P produced trabecular layers with higher porosity, broader pore distributions, and more biomimetic architecture compared to the conventional sintering approach, highlighting the superior osteointegration potential in constructs made by I3P. Abbreviations: CS, Cast-sintered; I3P, integrated 3D printing.

trabecular and laminar structures in a single process. With I3P, the production workflow is unified and streamlined, eliminating uncertainties associated with multistep processes, such as sintering or plasma spraying, as well as the conventional additive manufacturing methods, which is particularly beneficial for industrial-scale production. I3P also offers unmatched controllability over product properties and allows patient-specific customization, a key advantage in the context of future clinical practice that increasingly emphasizes individualized implants.

4.1. Substrate characteristics

From a substrate perspective, I3P substrates exhibit refined and homogeneous grain structures that conventional casting cannot achieve. Although forging can partly compensate for the deficiencies of cast alloys, the brittleness of CoCrMo and irregular casting porosity make such improvements technically challenging and costly. I3P using LPBF may display anisotropy due to directional grain growth (Figure 2). However, this study showed that optimized processing, such as HIP, minimized such anisotropy, resulting in no pronounced texture in the grain structures (Figure 2). This translated to improved material characteristics such as yield strength and ultimate tensile strength that surpassed the corresponding conventional cast implants (Figure 2). This microstructural refinement was directly linked to superior mechanical properties.

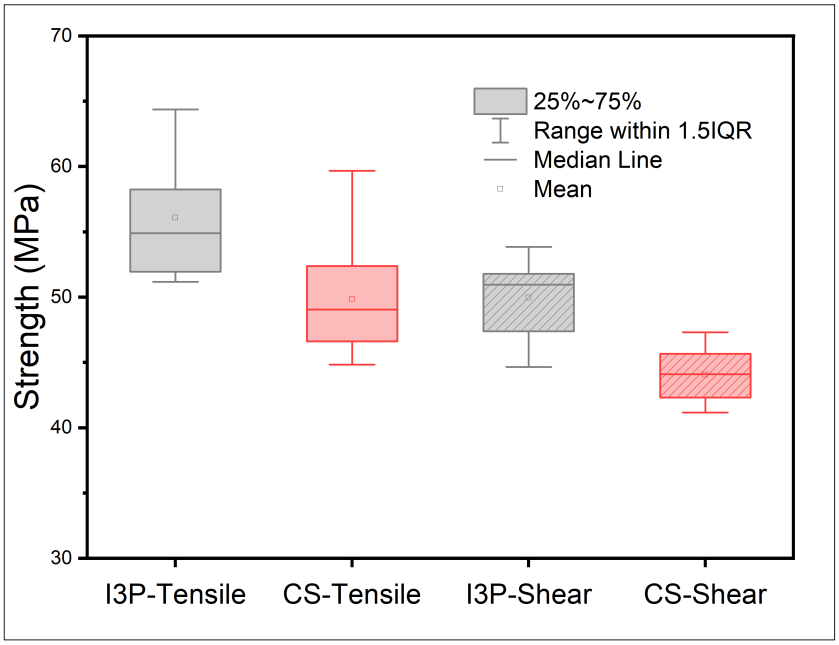

Figure 6. Interfacial bonding strength between trabecula-inspired porous layers and substrates fabricated by I3P and CS. Tensile and shear bond strength were measured using a universal testing machine with 10 specimens per group. I3P structures demonstrated significantly higher values (tensile: 56.1 MPa; shear: 50.0 MPa) compared with sintered counterparts, reflecting the advantage of forming the porous layer and substrate in a single integrated step. In contrast, sintered structures are prone to incomplete melting and nonuniform particle necking, which weakens the interface. The superior bonding performance of I3P establishes a more durable and reliable substrate–porous junction, reducing risks of delamination and enhancing long-term implant stability. *Compared with the CS specimens, the I3P specimens showed two-sample Student's *t*-test *p*-values of 7.41×10^{-3} for tensile strength. **Compared with the CS specimens, the I3P specimens showed two-sample Student's *t*-test *p*-values of 4.67×10^{-5} for shear strength. Abbreviations: CS: Cast-sintered; I3P: integrated 3D printing.

The improvement in mechanical properties and its connection with microstructural refinement is clearly highlighted by the quantitative tensile testing. Prior to HIP, I3P substrates showed mixed performance when compared with cast substrates. However, after HIP the I3P substrates significantly outperformed the cast counterparts in yield strength, tensile strength, and ductility (Figure 3). This demonstrates the central importance of eliminating micropores and residual interlayer defects from LPBF (Figure 2) through an optimized HIP process.

This microstructure refinement also improves wear and fatigue resistance. The finer microstructure of I3P alloys translated into superior hardness (31 HRC vs. 23 HRC for cast), enabling smoother polishing and reduced counterface wear. In long-term wear testing up to 5 million cycles, I3P femoral condyles consistently showed lower mass loss compared to cast controls (Figure 3). This performance reflects both higher intrinsic hardness and the reduced local hardness variability afforded by the uniform I3P microstructure. Cast alloys, by contrast, contain microstructural inhomogeneities that limit surface smoothness and accelerate tibial insert wear.

Finally, in terms of fatigue resistance, I3P femoral condyles demonstrated superior performance, surviving at least 10 million cycles at 3000 N, compared with 2900 N for cast femoral condyles (Figure 4). At each step increase in load, I3P specimens maintained a higher survival rate and endured more cycles before failure. This improved fatigue performance is attributed to the homogeneity of the I3P substrate, which distributes applied stresses more uniformly, thereby reducing stress concentrations that typically initiate cracks in coarser cast alloys.

Taken together, I3P substrates feature a refined grain structure, higher tensile strength and ductility after HIP, greater hardness and wear resistance, and improved fatigue life, as compared with conventionally cast substrates. These attributes confer superior durability and risk resistance, supporting I3P as a promising manufacturing route for cementless femoral condyles.

Trabecular surface characteristics

The bone-contacting surface of a cementless femoral condyle implant is central to its clinical performance, as both the pore architecture and the integrity of the substrate–porous interface determines osteointegration

and long-term mechanical stability. I3P can outperform conventional additive manufacturing methods in terms of interfacial bonding strength, and has demonstrated clear advantages over traditional sintering in both respects.

CT-based characterization revealed that I3P trabeculations were formed with thinner mean struts and substantially higher porosity (67.6% vs. 40.5%) (Figure 5). These characteristics are directly favorable for osteointegration, since increased porosity and reduced strut thickness enhance surface area for bone apposition while providing more open channels for vascular and cellular infiltration. The mean pore size of I3P trabeculae (317.2 ± 124.4 μm) was more than twice that of sintered layers (141.6 ± 49.2 μm), placing it firmly within the widely recognized 100–500 μm window for bone ingrowth (Figure 5).[27] Importantly, the broader pore size distribution produced by I3P offers additional biological advantages: smaller pores can facilitate early osteoid deposition and cell adhesion, while larger pores accommodate neovascularization and subsequent bone remodeling.[28–31] By contrast, the narrower pore size distribution of sintered coatings are constrained by bead diameter and stacking behavior. This limits biological adaptability and does not recapitulate the morphological heterogeneity of native trabecular bone. Together, these findings underscore I3P's capacity to produce pore architectures that are not only within the optimal osteoconductive range but also more biomimetic and adaptable across different phases of bone healing.

The integrity of the interface between the porous layer and the dense substrate is equally critical to implant performance, as failures often occur by delamination or particle shedding. Mechanical testing confirmed that I3P generated a stronger and more reliable interface compared to those of sintered counterparts (Figure 6). This difference arises from fundamental differences in process physics. In sintering, discrete beads fuse through neck formation that is often incomplete or nonuniform, leaving weak links at both bead–bead junctions and at the porous–substrate boundary. This random packing and limited metallurgical continuity elevate the risk of interface separation under cyclic load. By contrast, I3P builds the porous trabeculae and solid substrate in a single integrated step, ensuring full material continuity and densification across the transition zone. Even though the average I3P struts are thinner than sintered beads, the absence of incomplete melting or weak necks produces a far stronger and more stable bond. This continuity translates into lower delamination risk, higher structural reliability, and longer-term stability of the implant surface *in vivo*.

Structurally, the trabecula-inspired porous layers generated by I3P not only provide superior control over porosity and interconnectivity but also enable precise tailoring of these parameters to match biological and mechanical requirements. The ability to adjust pore size distribution, strut thickness, and layer thickness within a controlled design framework opens opportunities for patient-specific implants optimized for anatomical site, bone quality, or activity level. Moreover, the integration of porous and dense regions in a single build eliminates the delamination and particle shedding risks inherent in sintered or mechanically bonded coatings. These combined features support more effective osteointegration and more durable long-term fixation, underscoring the clinical potential of I3P as a next-generation manufacturing approach for cementless femoral condyle implants.

4.3. Clinical significance and future directions

Taken together, I3P femoral condyles unite three essential performance attributes: a substrate with refined microstructure and superior mechanical strength to withstand abnormal stresses, enhanced hardness and fatigue resistance to extend service life, and a trabecula-inspired porous layer optimized for osteointegration. This unique triad positions I3P as a superior alternative to conventional additive manufacturing and to casting-and-sintering approaches, particularly for cementless fixation where both mechanical integrity and biological integration are critical.[32]

At the same time, product-level outcomes remain influenced by implant geometry and patient-specific variables such as anatomy, activity level, and bone quality. The present study addressed this variability by employing the worst-case model by a head-to-head using a particular commercial implant geometry, thereby ensuring that the comparative results are both stringent and representative. With its structural precision and flexibility, I3P is expected to deliver even greater adaptability and performance across a wider spectrum of implant geometries and patient conditions.

Although the present study focused on mechanical and structural performance of I3P, the biological response to I3P surfaces is an important direction of future work. *In vitro* and *in vivo* studies examining osteoblast adhesion, bone ingrowth, and interfacial remodeling complement the mechanical findings reported here. Prior investigations of lattice architectures with comparable pore size and interconnectivity have demonstrated favorable osteoconductive behavior, suggesting similar potential for the I3P trabecular surfaces described in this study. Future work will address detailed evaluation of these biological aspects.

Beyond the knee, the intrinsic versatility of I3P supports translation of this approach to other load-bearing and articulating systems, including hip, shoulder, and wrist implants, as well as spinal devices. Based on the advantages demonstrated here, I3P holds promise to improve fixation, durability, and long-term stability across multiple orthopedic applications, reinforcing its potential as a scalable platform technology for next-generation implant design.

5. Conclusion

This study demonstrates the advantages of I3P in the fabrication of cementless femoral condyles through a comprehensive evaluation of its substrate- and product-level performance compared with conventional manufacturing routes. I3P substrates exhibited finer and more homogeneous microstructures than cast or sintered alloys, resulting in superior tensile properties, improved fatigue resistance, and greater hardness that allowed smoother polishing and reduced counterface wear. At the surface level, I3P outperformed sintering by producing trabecula-inspired structures with controllable pore size distribution, enhanced interconnectivity, and stronger bonding to the substrate. Together, these attributes highlight I3P as a robust platform for extending implant longevity and improving biological integration.

The intrinsic flexibility and precision of additive manufacturing further positions I3P as a versatile tool for optimizing implant design according to patient-specific anatomy and *in vivo* loading conditions, enabling iterative advances toward personalized solutions for even primary procedures. The integrated nature of the process also ensures product stability, underscoring its scalability for industrial production and clinical translation. While this work focused on femoral condyles, the same principles can be extended to hip, shoulder, and wrist implants, as well as spinal systems. Collectively, these findings establish a foundation for the broader application of I3P in cementless arthroplasty and support its potential as a next-generation strategy in orthopedic implant manufacturing.

Acknowledgments

None.

Funding

All materials, products, equipment, and funding for this study were provided by Suzhou Microport Orthorecon Co., Ltd.

Conflict of interest

J.W., Z.Z., T.Y., and W.W. are employees of Suzhou Microport Orthorecon, a subsidiary of MicroPort Orthopedics which produces and markets the commercial EVOLUTION femoral condyle implant examined in this study. B.Y.C. is an employee of MicroPort at the time of publication of this work.

Author contributions

Conceptualization: Tianbai Yu, Jiawei Wu, Zhiwei Zhou, Brian Chang
Formal analysis: Jiawei Wu, Zhiwei Zhou
Investigation: Zhiwei Zhou, Jiawei Wu
Methodology: Zhiwei Zhou, Jiawei Wu, Wei Wang
Writing–original draft: Jiawei Wu, Zhiwei Zhou
Writing–review & editing: Zhiwei Zhou, Jiawei Wu, Brian Chang

Ethics approval and consent to participate

Not applicable.

Consent for publication

Not applicable.

Availability of data

The datasets generated and/or analyzed during the current study are partially available from the corresponding author upon reasonable request. Certain data are subject to corporate confidentiality restrictions and therefore cannot be made publicly available.

References

1. Batailler C, Swan J, Sappey Marinier E, Servien E, Lustig S. New technologies in knee arthroplasty: Current concepts. *J Clin Med*. 2020;10(1):47. doi: 10.3390/jcm10010047
2. Mukartihal R, Das R, Chandan S, *et al*. Technologies in total knee arthroplasty. *J Karnataka Orth Assc*. 2023; 11(1):5-12. doi: 10.13107/jkoa.2023.v11i01.057
3. Prakash R, Agrawal Y. Robotic technology in total knee arthroplasty. *Br J Hosp Med*. 2023;84(6):1-9. doi: 10.12968/hmed.2022.0491
4. Haslhofer DJ, Kraml N, Stadler C, Gotterbarm T, Klotz MC, Klasan A. Cementless fixation in total knee arthroplasty: Current evidence and future perspective. *Arch Orthop Trauma Surg*. 2024;145(1):101. doi: 10.1007/s00402-024-05670-2

5. Lohberger B, Eck N, Glaenzer D, Lichtenegger H, Ploszczanski L, Leithner A. Cobalt chromium molybdenum surface modifications alter the osteogenic differentiation potential of human mesenchymal stem cells. *Materials (Basel)*. 2020;13(19):4292.
doi: 10.3390/ma13194292

6. Anselme K, Linez P, Bigerelle M, *et al*. The relative influence of the topography and chemistry of TiAl6V4 surfaces on osteoblastic cell behaviour. *Biomaterials*. 2000;21(15):1567-1577.
doi: 10.1016/S0142-9612(00)00042-9

7. Logan N, Sherif A, Cross AJ, *et al*. TiO_2-coated CoCrMo: Improving the osteogenic differentiation and adhesion of mesenchymal stem cells *in vitro*. *J Biomed Mater Res*. 2015;103(3):1208-1217.
doi: 10.1002/jbm.a.35264

8. Saroya M, Singh N, Singh A. Thermal spray coating technology – A review. *Int J Multidiscip Res*. 2023;5(3):2990.
doi: 10.36948/ijfmr.2023.v05i03.2990

9. Heimann RB. Thermal spraying of biomaterials. *Surf Coat Technol*. 2006;201(5):2012-2019.
doi: 10.1016/j.surfcoat.2006.04.052

10. Kumari R, Majumdar JD. Microstructure and surface mechanical properties of plasma spray deposited and post spray heat treated hydroxyapatite (HA) based composite coating on titanium alloy (Ti-6Al-4V) substrate. *Mater Charact*. 2017;131:12-20.
doi: 10.1016/j.matchar.2017.06.011

11. Mittal M, Nath S, Prakash S. Splat formation and degradation of hydroxyapatite during plasma spraying process. *Adv Mater Sci*. 2011;11(2).
doi: 10.2478/v10077-011-0008-6

12. Patel B, Inam F, Reece M, *et al*. A novel route for processing cobalt–chromium–molybdenum orthopaedic alloys. *J R Soc Interface*. 2010;7(52):1641-1645.
doi: 10.1098/rsif.2010.0036

13. Minouei H, Fathi M, Meratin M, Ghazvinizadeh H. Heat treatment of cobalt-base alloy surgical implants with hydroxyapatite-bioglass for surface bioactivation. *Iran J Mater Sci Eng*. 2012;9(3):33-39.

14. Das A, Rajkumar P. Metal 3D printing of biometals for prostheses and implants: A review. *Explor BioMat X*. 2025;2:101338.
doi: 10.37349/ebmx.2025.101338

15. Chowdhury S, Yadaiah N, Prakash C, *et al*. Laser powder bed fusion: A state-of-the-art review of the technology, materials, properties & defects, and numerical modelling. *J Mater Res Technol*. 2022;20:2109-2172.
doi: 10.1016/j.jmrt.2022.07.121

16. Archaryagie KCS, Tang Y. Enhancing powder bed quality in laser powder bed fusion: A review of monitoring, data processing, and adaptive control strategies. *J Manuf Process*. 2025;149:276-304.
doi: 10.1016/j.jmapro.2025.05.058

17. Walker J, Middendorf JR, Lesko CCC, Gockel J. Multi-material laser powder bed fusion additive manufacturing in 3-dimensions. *Manuf Lett*. 2022;31:74-77.
doi: 10.1016/j.mfglet.2021.07.011

18. Hasan N, Habibor Rahman M, Wessman A, Smith T, Shafae M. Process defects knowledge modeling in laser powder bed fusion additive manufacturing: An ontological framework. *Manuf Lett*. 2023;35:822-833.
doi: 10.1016/j.mfglet.2023.08.132

19. Sandu AV, Baltatu MS, Nabialek M, Savin A, Vizureanu P. Characterization and mechanical proprieties of new TiMo alloys used for medical applications. *Materials (Basel)*. 2019;12(18):2973.
doi: 10.3390/ma12182973

20. Baltatu MS, Tugui CA, Perju MC, *et al*. Biocompatible titanium alloys used in medical applications. *Rev Chim*. 2019;70(4):1302-1306.
doi: 10.37358/RC.19.4.7114

21. Jiao J, Hong Q, Zhang D, *et al*. Influence of porosity on osteogenesis, bone growth and osteointegration in trabecular tantalum scaffolds fabricated by additive manufacturing. *Front Bioeng Biotechnol*. 2023;11:1117954.
doi: 10.3389/fbioe.2023.1117954

22. Zhou Y, Ning F, Zhang P, Sharma A. Geometrical, microstructural, and mechanical properties of curved-surface AlSi10Mg parts fabricated by powder bed fusion additive manufacturing. *Mater Des*. 2021;198:109360.
doi: 10.1016/j.matdes.2020.109360

23. Ramavath D, Yeole SN, Kode JP, Pothula N, Devana SR. Development of patient-specific 3D printed implants for total knee arthroplasty. *Explor Med*. Published online December 28, 2023:1033-1047.
doi: 10.37349/emed.2023.00193

24. Velásquez-García LF, Kornbluth Y. Biomedical applications of metal 3D printing. *Annu Rev Biomed Eng*. 2021;23(1):307-338.
doi: 10.1146/annurev-bioeng-082020-032402

25. Chowdhury MS, Oliullah MS, Hossen MZ, *et al*. Additive manufacturing in bone science: A cutting-edge review of its potential and progress. *Med Nov Technol Devices*. 2025;27:100379.
doi: 10.1016/j.medntd.2025.100379

26. Li Y, Jiang D, Zhu R, Yang C, Wang L, Zhang LC. Revolutionizing medical implant fabrication: Advances in additive manufacturing of biomedical metals. *Int J Extrem Manuf*. 2025;7(2):022002.
doi: 10.1088/2631-7990/ad92cc

27. Li G, Wang L, Pan W, *et al*. In vitro and in vivo study of additive manufactured porous Ti6Al4V scaffolds for repairing bone defects. *Sci Rep*. 2016;6(1):34072. doi: 10.1038/srep34072

28. Otsuki B, Takemoto M, Fujibayashi S, Neo M, Kokubo T, Nakamura T. Pore throat size and connectivity determine bone and tissue ingrowth into porous implants: Three-dimensional micro-CT based structural analyses of porous bioactive titanium implants. *Biomaterials*. 2006;27(35):5892-5900. doi: 10.1016/j.biomaterials.2006.08.013

29. Wang X, Zhang D, Peng H, Yang J, Li Y, Xu J. Optimize the pore size-pore distribution-pore geometry-porosity of 3D-printed porous tantalum to obtain optimal critical bone defect repair capability. *Biomater Adv*. 2023;154:213638. doi: 10.1016/j.bioadv.2023.213638

30. Jones A, Arns C, Sheppard A, Hutmacher D, Milthorpe B, Knackstedt M. Assessment of bone ingrowth into porous biomaterials using MICRO-CT. *Biomaterials*. 2007;28(15):2491-2504. doi: 10.1016/j.biomaterials.2007.01.046

31. Li J, Yang Y, Sun Z, *et al*. Integrated evaluation of biomechanical and biological properties of the biomimetic structural bone scaffold: Biomechanics, simulation analysis, and osteogenesis. *Materials Today Bio*. 2024;24:100934. doi: 10.1016/j.mtbio.2023.100934

32. Qu Z, Yue J, Song N, Li S. Innovations in three-dimensional-printed individualized bone prosthesis materials: Revolutionizing orthopedic surgery: A review. *Int J Surg*. 2024;110(10):6748-6762. doi: 10.1097/JS9.0000000000001842